CHEMISTRY
A EUROPEAN JOURNAL

DOI: 10.1002/chem.200501534

Triphenylantimony(v) Catecholates and *o*-Amidophenolates: Reversible Binding of Molecular Oxygen

Vladimir K. Cherkasov, Gleb A. Abakumov,* Ekaterina V. Grunova, Andrey I. Poddel'sky, Georgy K. Fukin, Evgenii V. Baranov, Yury V. Kurskii, and Ludmila G. Abakumova[a]

Abstract: Novel neutral antimony(v) complexes were isolated as crystalline materials and characterized by IR and NMR spectroscopy: *o*-amidophenolate complexes [4,6-di-*tert*-butyl-*N*-(2,6-dimethylphenyl)-*o*-amidophenolato]triphenylantimony(v) (Ph_3Sb[AP-Me], **1**) and [4,6-di-*tert*-butyl-*N*-(2,6-diisopropylphenyl)-*o*-amidophenolato]triphenylantimony(v) (Ph_3Sb[AP-*i*Pr], **2**); catecholate complexes (3,6-di-*tert*-butyl-4-methoxycatecholato)triphenylantimony(v) (Ph_3Sb[(MeO)Cat], **3**), its methanol solvate **3**·CH_3OH (**4**); (3,6-di-*tert*-butyl-4,5-di-methoxycatecholato)triphenylantimony(v) (Ph_3Sb[$(MeO)_2$Cat], **5**) and its acetonitrile solvate **5**·CH_3CN (**6**). Complexes **1**–**7** were synthesized by oxidative addition of the corresponding *o*-iminobenzoquinones or *o*-benzoquinones to Ph_3Sb. In the case of the phenanthrene-9,10-diolate (PhenCat) ligand, two different complexes were isolated: Ph_3Sb[PhenCat] (**7**) and $[Ph_4Sb]^+[Ph_2Sb(PhenCat)_2]^-$ (**8**). Complexes **7** and **8** were found to be in equilibrium in solution. Molecular structures of **2**, **4**, **6**, and **8** were determined by X-ray crystallography. Complexes **1**–**7** reversibly bind molecular oxygen to yield Ph_3Sb[L-Me]O_2 (**9**), Ph_3Sb[L-*i*Pr]O_2 (**10**), Ph_3Sb-[(MeO)L′]O_2 (**11**), Ph_3Sb[$(MeO)_2$L′]O_2 (**12**) and Ph_3Sb[PhenL′]O_2 (**13**), which contain five-membered trioxastibolane species (where L is the O,O′,N-coordinated derivative of a 1-hydroperoxy-6-(*N*-aryl)-iminocyclohexa-2,4-dienol, and L′ the O,O′,O″-coordinated derivative of 6-hydroperoxy-6-hydroxycyclohexa-2,4-dienone). Complexes **9**–**13** were characterized by IR and ^1H NMR spectroscopy and X-ray crystallography.

Keywords: antimony · chelates · N,O ligands · O ligands · oxygenation

Introduction

The fixation of dioxygen in the coordination sphere of metal atoms is a subject of extreme interest due to its utilization by biological systems.[1] Dioxygen, although a powerful oxidizing agent, is kinetically inert, and in general requires activation by binding to a reduced metal center. The multitude of biological compounds that react with O_2 are either dioxygen enzymes in biological oxygen-involving processes or the transporters and storers of dioxygen. Elsewhere in biological processes, activation of molecular oxygen occurs by coordination in metalloproteins that catalyze oxygen insertion reactions and oxidation. The development of redox processes in biochemistry and technology requires synthetic analogues of natural dioxygen carriers. The biological utilization of dioxygen has led to an additional interest in the investigation of many, much simpler, model systems.

A wide range of transition-metal complexes will bind dioxygen reversibly.[2] However, in many cases the realization of this process needs a combination of certain conditions such as low temperature, steric hindrance in the complexes and immobilization to prevent irreversible oxidation of dioxygen adducts.[3] The search for stable transporters and carriers of O_2 maintains its importance.

In all cases of dioxygen binding by transition-metal complexes, electron transfer takes place from the redox-active transition metal to the antibonding π orbitals of the bound dioxygen. Recently, we found that replacing redox-active metal centers with redox-active organic ligands in complexes may also result in O_2-active reagents. Our preliminarily report was on the first example of reversible dioxygen bind-

[a] Prof. Dr. V. K. Cherkasov, Prof. Dr. G. A. Abakumov, E. V. Grunova, Dr. A. I. Poddel'sky, Dr. G. K. Fukin, E. V. Baranov, Dr. Y. V. Kurskii, Dr. L. G. Abakumova
G. A. Razuvaev Institute of Organometallic Chemistry
Russian Academy of Sciences
49 Tropinina Street, 603950 Nizhny Novgorod (Russia)
Fax: (+7) 8312-62-74-97
E-mail: cherkasov@imoc.sinn.ru
aip@imoc.sinn.ru

ing by a non-transition-metal complex, namely, *o*-amidophenolatotriphenylantimony(v) **2**.[4] The unique ability of **2** to bind dioxygen reversibly was found to be due to the redox activity of the *o*-amidophenolate ligand. *o*-Amidophenolate dianions AP^{2-} undergo reversible single-electron oxidation to *o*-iminobenzosemiquinolates in the coordination sphere of a metal center.[5] The suggested mechanism of dioxygen binding assumes one-electron oxidation of *o*-amidophenolate dianionic to *o*-iminobenzosemiquinolate radical-anionic ligand.[4] The redox potential of conversion from dianionic ligand (catecholate or *o*-amidophenolate) to radical anion (*o*-semiquinolate or *o*-iminobenzosemiquinolate) plays the crucial role in forbidding or allowing the dioxygen binding process. Proof of this mechanism is the ability of (4,5-dimethoxy-3,6-di-*tert*-butyl-catecholato)triphenylantimony(v) and (4-methoxy-3,6-di-*tert*-butylcatecholato)triphenylantimony(v) to reversibly bind dioxygen. Due to the electron-donor character of the methoxyl groups, the catecholate ligands in these complexes are more easily oxidized than unsubstituted 3,6-di-*tert*-butyl-catecholato)triphenylantimony(v), which does not interact with dioxygen to form an endoperoxide.[6]

This report focuses on the synthesis of novel triphenylantimony(v) catecholates and *o*-amidophenolates with different redox potentials for catecholate→*o*-semiquinolate (or *o*-amidophenolate→*o*-iminobenzosemiquinolate) conversion and their capability to reversibly bind dioxygen.

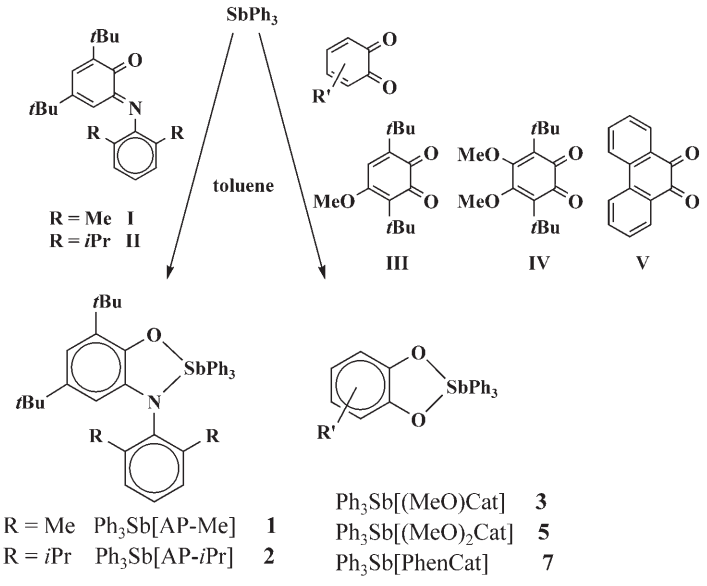

Scheme 1.

Results and Discussion

Synthesis and characterization of triphenylantimony(v) catecholates and *o*-amidophenolates: *o*-Amidophenolate triphenylantimony complexes **1** and **2**, and catecholate triphenylantimony complexes **3**–**7** were prepared by oxidative addition reaction of triphenylantimony with the corresponding *o*-iminobenzoquinones 4,6-di-*tert*-butyl-*N*-(2,6-di-methylphenyl)-*o*-iminobenzoquinone (IBQ-Me, **I**) and 4,6-di-*tert*-butyl-*N*-(2,6-diisopropylphenyl)-*o*-iminobenzoquinone (IBQ-*i*Pr, **II**),[4] or *o*-benzoquinones 4-methoxy-3,6-di-*tert*-butyl-*o*-benzoquinone (4-MeO-3,6-DBBQ, **III**), 4,5-di-methoxy-3,6-di-*tert*-butyl-*o*-quinone (4,5-$(MeO)_2$-3,6-DBBQ, **IV**)[7] and 9,10-phenanthrenequinone (**V**) at ambient temperature in toluene solution (Scheme 1).

Slow evaporation of solutions of **1**–**3** and **5** in toluene afforded microcrystalline materials that were identified by IR, ^{1}H NMR, and UV/Vis spectroscopy and elemental analysis. Slow recrystallization of **3** from methanol gave six-coordinate antimony(v) compound **3**·CH_3OH (**4**); recrystallization of **5** from acetonitrile gave **5**·CH_3CN (**6**).

In deaerated toluene solution phenanthrene-9,10-diolate **7** exists in equilibrium with complex ionic form $[Ph_4Sb]^+[Ph_2Sb(PhenCat)_2]^-$ (**8**; Scheme 2). The formation of $[Ph_4Sb]^+$ ions and antimonate anions is well known. For example, the reaction between triphenylantimony dichloride and silver oxalate depends on both the solvent and temperature; thus, after refluxing the toluene solution, crystals of $[Ph_4Sb]^+[Ph_2Sb(ox)_2]^-$ [ox = oxalate(2−)] an ionic form of $SbPh_3(ox)$, are obtained at room temperature.[8]

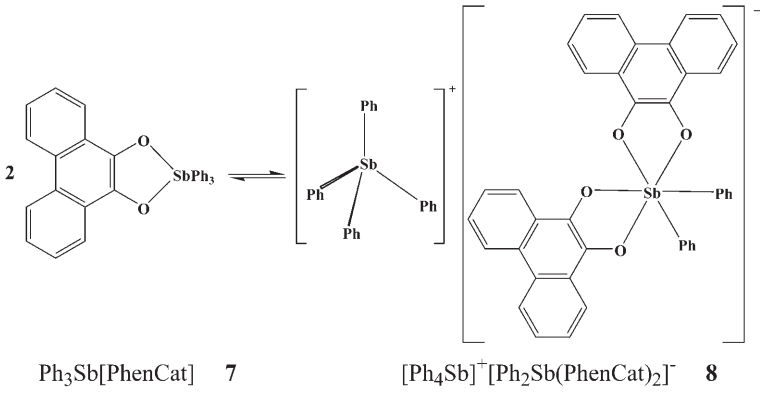

Scheme 2.

IR spectroscopic data confirm the proposed *o*-amidophenolate structure of **1** and **2** and catecholate structure of **3**–**8**.

Crystal structures of 2, 4, 6 and 8: The crystal structures of **2**, **4**, **6**, and **8** were determined by single-crystal X-ray diffraction. Molecular structures of **4**, **6**, and **8** are depicted in Figures 1–3. Crystallographic data and details of structure

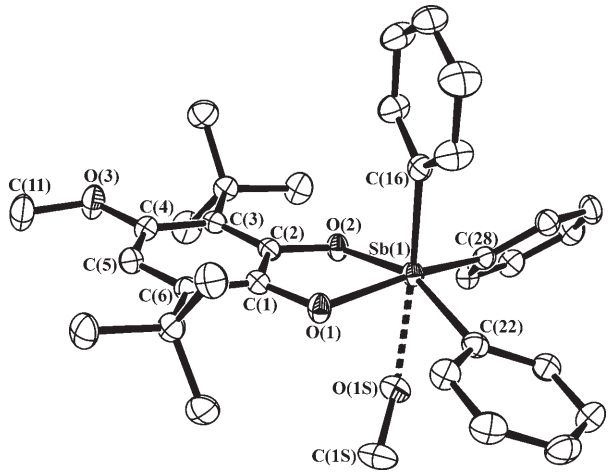

Figure 1. An ORTEP view of **4** with 50% probability ellipsoids (H atoms omitted).

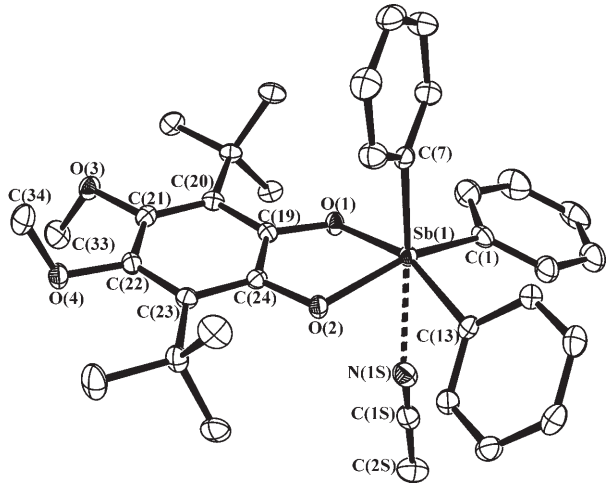

Figure 2. An ORTEP view of **6** with 50% probability ellipsoids (H atoms omitted).

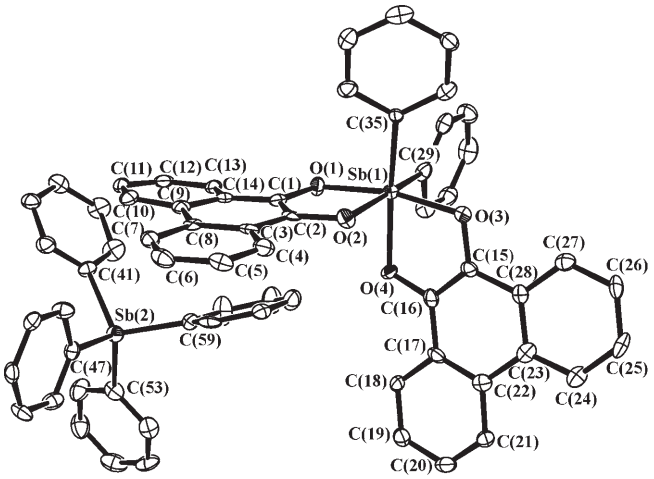

Figure 3. An ORTEP view of **8** with 50% probability ellipsoids (H atoms omitted).

determination are given in Table 1; Tables 2–4 summarize selected bond lengths and angles.

Single crystals of **2** suitable for X-ray analysis were obtained by slow recrystallization from toluene as toluene solvate **1**·0.5 $C_6H_5CH_3$. The molecular structure of **2** was described previously.[4] The Sb(1) atom has a distorted tetragonal-pyramidal environment. The structure determination unambiguously showed that **2** is an antimony(v) complex of an *o*-amidophenolate dianion and three phenyl groups. Since the spectroscopic data of complexes **1** and **2** are similar, we consider the molecular structure of **1** to be close to that of **2**.

According to X-ray diffraction analysis, Sb atoms in complexes **4** and **6** are six-coordinate and have a distorted octahedral environment. The Sb atoms in **4** and **6** are coordinated by donor molecules S (S = MeOH for **4** and S = MeCN for **6**). The catecholate fragment and two phenyl groups lie in the equatorial plane. The third phenyl group and donor atom of S occupy axial positions. The displacement of the Sb atom from the basal plane in the direction toward the axial phenyl group is 0.328 Å in **4** and 0.362 Å in **6**. The angles between equatorial and axial substituents vary in the ranges of 96.24(4)–105.14(5) and 175.61(4)–177.06(3)°, respectively. The sum of angles O-Sb-O, O-Sb-Ph, and Ph-Sb-Ph in the equatorial plane is 354.3° in **4** and 353.48° in **6**. The five-membered metallocycles in **4** and **6** are not planar. The bending angles along the O···O vector are 16.8° for **4** and 16.6° for **6** and are the largest among similar complexes.

The Sb(1)–O(1,2) bond lengths in **4** are nearly equal (2.030(1) and 2.028(1) Å), whereas in **6** they are slightly different (2.033(1) and 2.017(1) Å). The C(1)–O(1), C(2)–O(2) distances in **4** and C(19)–C(1), C(24)–C(2) distances in **6** are 1.357(2) and 1.355(2) Å, 1.361(2) and 1.361(1) Å, respectively, and they are typical catecholate bond lengths (1.35–1.38 Å).[6,9,10] The Sb–C_{Ph} bond lengths are in the range of 2.117(1)–2.145(1) Å for both **4** and **6**. The Sb···O (in **4**) and Sb···N (in **6**) distances of the donor–acceptor bonds are 2.461(1) and 2.775(1) Å, respectively. A correlation exists between the Sb···O and Sb···N distances and the ionization potentials of the coordinated molecules in complexes **4** and **6** ($E(MeOH)_{ion} = 10.85$, $E(MeCN)_{ion} = 12.12$ eV).[11]

Crystals of **8** contain one CH_2Cl_2 molecule of solvation per molecule of complex. The complex consists of a tetrahedral tetraphenylantimony(v) cation and an octahedral bis-(phenanthrene-9,10-diolate)diphenylantimonate(v) anion. The Sb–C distances in the cation lie in the range of 2.074(5)–2.104(5) Å and are close to the corresponding bond lengths in the cation of the similar compound $[Ph_4Sb]^+$ $[Ph_2Sb(ox)_2]^-$ [ox = oxalate(2–)] (2.09 Å).[8]

The phenyl groups in the anion occupy *cis* positions (C(35)-Sb(1)-C(29) 100.9(2)°), with Sb–C bond lengths of 2.128(5) and 2.138(5) Å, somewhat longer than those in the cation. The phenanthrene-9,10-diolate ligands coordinate to the Sb atom slightly unsymmetrically. The Sb(1)–O(1,2) and Sb(1)–O(3,4) distances in the ligands are 2.030(3), 2.072(3) Å and 2.031(3), 2.069(3) Å, respectively. The Sb(1)–O(1) and Sb(1)–O(3) bonds are located in *trans* positions relative to each other, whereas the Sb(1)–O(2) and

Table 1. Summary of crystal and refinement data for **4**, **6**, and **8**.

	$Ph_3Sb[(MeO)Cat]\cdot CH_3OH$ (**4**)	$Ph_3Sb[(MeO)_2Cat]\cdot CH_3CN$ (**6**)	$[Ph_4Sb]^+[Ph_2Sb(PhenCat)_2]^-$ (**8**)
empirical formula	$C_{36}H_{49}O_6Sb$	$C_{36}H_{42}O_4NSb$	$C_{65}H_{48}Cl_2O_4Sb_2$
formula weight	699.49	674.46	1207.43
temperature [K]	100(2)	100(2)	100(2)
wavelength [Å]	0.71073	0.71073	0.71073
crystal system	monoclinic	monoclinic	monoclinic
space group	*c*2/*c*	*P*2(1)/*n*	*P*2(1)
a [Å]	35.0856(15)	13.5746(6)	9.6865(6)
b [Å]	10.7380(5)	15.9506(7)	21.2953(12)
c [Å]	17.9922(8)	15.0855(7)	13.1638(8)
α [°]	90	90	90
β [°]	98.4000(10)	97.8410(10)	109.7520(10)
γ [°]	90	90	90
V [Å^3]	6705.8(5)	3235.8(3)	2555.6(3)
Z	8	4	2
ρ_{calcd} [Mg m^{-3}]	1.354	1.384	1.569
absorption coefficient [mm^{-1}]	0.863	0.891	1.213
crystal size [mm]	0.20×0.13×0.08	0.84×0.38×0.35	0.29×0.19×0.02
reflections collected	18198	25015	14219
independent reflections	5909 [*R*(int) = 0.0165]	5673 [*R*(int) = 0.0144]	8806 [*R*(int) = 0.0398]
absorption correction	SADABS	SADABS	SADABS
max./min. transmission	0.9341/0.8463	0.7456/0.5214	0.9761/0.7198
refinement method	full-matrix least-squares on F^2	full-matrix least-squares on F^2	full-matrix least-squares on F^2
data/restraints/parameters	5909/2/570	5673/0/547	8806/13/658
final *R* indices[a] [$I>2\sigma(I)$]			
*R*1	0.0231	0.0175	0.0445
*wR*2	0.0632	0.0455	0.0780
R indices[a] (all data)			
*R*1	0.0258	0.0182	0.0577
*wR*2	0.0645	0.0458	0.0818
GOF[b] on F^2	1.066	1.097	1.088
largest diff. peak/hole [e Å^{-3}]	0.511/−0.460	0.383/−0.343	1.291/−0.524

[a] $R=\Sigma||F_o|-|F_c||/\Sigma|F_o|$; $wR=R(wF^2)=[\Sigma w(F_o^2-F_c^2)^2/\Sigma w(F_o^2)^2]^{1/2}$, $w=1/[\sigma^2(F_o^2)+(aP)^2+bP]$, $P=[2F_c^2+F_o^2]/3$. [b] $GOF=[\Sigma w(F_o^2-F_c^2)^2/(n-p)]^{1/2}$, where *n* is the number of reflections, and *p* the number of refined parameters.

Sb(1)−O(4) bonds are located in *cis* positions. The differences in lengths of the Sb(1)−O(1,3) and Sb(1)−O(2,4) bonds can be explained by the *trans* effect of phenyl groups, which are positioned *trans* to O(2) and O(4) and thus increase the corresponding Sb(1)−O(2,4) distances.

The C−O bond lengths are in the range of catecholate C−O bonds (1.34–1.38 Å).[6,9,10]

Reversible dioxygen binding by 1–7: Previously, we reported that complex **2** binds molecular oxygen reversibly in solution to give **10**, which has a five-membered trioxastibolane ring.[4] Complex **1** also has such capability and interacts with molecular oxygen to give **9** (Scheme 3).

The formation of complexes **9** and **10** is evident from changes in the NMR and electronic absorption spectra observed on prolonged exposure of solutions of **1** and **2** to air. In the ^{1}H NMR spectrum the intensity of all signals of **1** decreases with simultaneous increase of the intensity of resonances related to **9**. The shifts of signals attributed to the *tert*-butyl and aromatic protons of a distorted *o*-amidophenolato group are observed on addition of dioxygen. The *tert*-butyl protons of **1** appear as two singlets at $\delta=1.15$ and 1.49 ppm, while those of **9** are found at $\delta=1.02$ and 1.36 ppm in $CDCl_3$. The signals of two aromatic protons of the amidophenolato ligand in **1** appear as a pair of doublets centered at $\delta=5.87$ and 6.75 ppm (^4J(H,H) = 2.3 Hz). The same protons of **9** give rise to doublets centered at $\delta=5.42$ and 6.48 ppm (^4J(H,H) = 1.6 Hz). Furthermore, in contrast to **1** the asymmetry of complex **9** produces inequivalence of two methyl protons of *N*-aryl substituents. Two methyl protons of **1** appear as a singlet at $\delta=1.98$ ppm. However, these methyl protons in **9** appear as two singlets at $\delta=$ 1.15 and 1.45 ppm. The ^{1}H NMR spectrum shows that full conversion of **1** and **2** to **9** and **10**, respectively, in [D$_6$]acetone solution (2×10^{-3} M) takes about 1 h in air. Repeated "freeze–pump (to remove molecular oxygen)–warm (to 50 °C)" cycles proved the reversibility of dioxygen binding by **1** and **2**.

Catecholate complexes **3–6** also interact with molecular oxygen reversibly to give **11** and **12** (Scheme 4).

The changes in the ^{1}H NMR spectrum observed on prolonged exposure of the solution of **3** to air were described earlier.[7] In the ^{1}H NMR spectrum (Figure 4) the intensity of all proton resonances of **3** and **5** decreases with immediate increase in intensity of resonances related to their molecular oxygen complexes **11** and **12**, respectively. Shifts of signals attributed to the *tert*-butyl and methoxyl protons are observed on addition of dioxygen to **3–6**. Thus, the *tert*-butyl protons of **5** appear as a singlet at $\delta=1.54$ ppm, while those of **12** are found at $\delta=1.29$ ppm in $CDCl_3$. The methoxyl protons of **5** appear as a singlet at $\delta=3.69$ ppm, while those of **12** are found at $\delta=3.73$ ppm. Repeated freeze–pump–warm cycles were used to prove the reversibility of dioxygen binding by complexes **3–6**.

Complex **7** also binds molecular oxygen reversibly to give complex $Ph_3Sb[PhenL']O_2$ (**13**).

The formation of complexes **9–13** is evident from a number of typical bands of their IR spectra in the range of

Table 2. Selected bond lengths [Å] and angles [°] for $Ph_3Sb[(MeO)Cat]\cdot CH_3OH$ (**4**).

Sb(1)–O(2)	2.0279(8)	O(2)-Sb(1)-O(1)	78.83(3)
Sb(1)–O(1)	2.0295(8)	O(2)-Sb(1)-C(16)	96.24(4)
Sb(1)–C(16)	2.1277(13)	O(1)-Sb(1)-C(16)	96.44(4)
Sb(1)–C(22)	2.1378(13)	O(2)-Sb(1)-C(22)	157.63(4)
Sb(1)–C(28)	2.1387(12)	O(1)-Sb(1)-C(22)	87.68(4)
Sb(1)–O(1S)	2.4615(10)	C(16)-Sb(1)-C(22)	102.99(5)
O(1)–C(1)	1.3574(15)	O(2)-Sb(1)-C(28)	85.08(4)
O(2)–C(2)	1.3548(15)	O(1)-Sb(1)-C(28)	158.55(4)
O(3)–C(4	1.3819(16)	C(16)-Sb(1)-C(28)	99.36(5)
O(3)–C(11)	1.4100(18)	C(22)-Sb(1)-C(28)	102.71(5)
C(1S)–O(1S)	1.4335(19)	O(2)-Sb(1)-O(1S)	79.91(3)
O(2S)–C(2S)	1.350(2)	O(1)-Sb(1)-O(1S)	80.80(3)
O(3S)–C(3S)	1.261(5)	C(16)-Sb(1)-O(1S)	175.61(4)
		C(22)-Sb(1)-O(1S)	80.38(4)
		C(28)-Sb(1)-O(1S)	82.50(4)
		C(1)-O(1)-Sb(1)	113.53(7)
		C(2)-O(2)-Sb(1)	114.63(7)
		C(17)-C(16)-Sb(1)	121.64(10)
		C(21)-C(16)-Sb(1)	119.34(10)
		C(23)-C(22)-Sb(1)	119.58(10)
		C(27)-C(22)-Sb(1)	121.40(10)
		C(29)-C(28)-Sb(1)	122.86(9)
		C(33)-C(28)-Sb(1)	117.77(9)
		C(1S)-O(1S)-Sb(1)	123.69(9)

Table 3. Selected bond lengths [Å] and angles [°] for $Ph_3Sb[(MeO)_2Cat]\cdot CH_3CN$ (**6**).

Sb(1)–O(2)	2.0173(8)	O(2)-Sb(1)-O(1)	78.76(3)
Sb(1)–O(1)	2.0334(8)	O(2)-Sb(1)-C(7)	99.39(4)
Sb(1)–C(7)	2.1166(12)	O(1)-Sb(1)-C(7)	94.46(4)
Sb(1)–C(1)	2.1332(12)	O(2)-Sb(1)-C(1)	152.80(4)
Sb(1)–C(13)	2.1451(12)	O(1)-Sb(1)-C(1)	87.70(4)
N(1)–C(1S)	1.1395(18)	C(7)-Sb(1)-C(1)	105.14(5)
O(1)–C(19)	1.3614(15)	O(2)-Sb(1)-C(13)	85.06(4)
O(2)–C(24)	1.3614(14)	O(1)-Sb(1)-C(13)	160.03(4)
O(3)–C(21)	1.3886(15)	C(7)-Sb(1)-C(13)	99.70(5)
O(3)–C(33)	1.4323(16)	C(1)-Sb(1)-C(13)	101.96(5)
O(4)–C(22)	1.3906(14)	C(19)-O(1)-Sb(1)	113.13(7)
O(4)–C(34)	1.4258(16)	C(24)-O(2)-Sb(1)	113.75(7)
C(1S)–C(2S)	1.459(2)	C(6)-C(1)-Sb(1)	118.48(10)
Sb(1)···N(1)	2.7750(12)	C(2)-C(1)-Sb(1)	121.85(10)
		C(8)-C(7)-Sb(1)	120.59(9)
		C(12)-C(7)-Sb(1)	120.09(9)
		C(18)-C(13)-Sb(1)	123.33(9)
		C(14)-C(13)-Sb(1)	117.18(9)

Table 4. Selected bond lengths [Å] and angles [°] for $[Ph_4Sb]^+$ $[Ph_2Sb(PhenCat)_2]^-$ (**8**).

Sb(1)–O(1)	2.030(3)	O(1)-Sb(1)-O(3)	168.17(14)
Sb(1)–O(3)	2.031(3)	O(1)-Sb(1)-O(4)	87.98(13)
Sb(1)–O(4)	2.069(3)	O(3)-Sb(1)-O(4)	81.07(13)
Sb(1)–O(2)	2.072(3)	O(1)-Sb(1)-O(2)	81.63(12)
Sb(1)–C(35)	2.128(5)	O(3)-Sb(1)-O(2)	92.49(13)
Sb(1)–C(29)	2.138(5)	O(4)-Sb(1)-O(2)	82.69(13)
O(1)–C(1)	1.375(6)	O(1)-Sb(1)-C(35)	100.47(15)
C(1)–C(2)	1.375(6)	O(3)-Sb(1)-C(35)	89.22(15)
C(1)–C(14)	1.421(6)	O(4)-Sb(1)-C(35)	164.33(15)
O(2)–C(2)	1.354(5)	O(2)-Sb(1)-C(35)	85.50(16)
C(2)–C(3)	1.429(7)	O(1)-Sb(1)-C(29)	90.03(16)
O(3)–C(15)	1.360(6)	O(3)-Sb(1)-C(29)	94.80(16)
C(3)–C(4)	1.419(7)	O(4)-Sb(1)-C(29)	92.15(17)
C(3)–C(8)	1.424(7)	O(2)-Sb(1)-C(29)	170.32(16)
O(4)–C(16)	1.345(6)	C(35)-Sb(1)-C(29)	100.9(2)
Sb(2)–C(59)	2.074(5)	C(1)-O(1)-Sb(1)	110.6(3)
Sb(2)–C(41)	2.097(5)	C(2)-O(2)-Sb(1)	110.4(3)
Sb(2)–C(47)	2.101(5)	C(15)-O(3)-Sb(1)	110.1(3)
Sb(2)–C(53)	2.104(5)	C(16)-O(4)-Sb(1)	110.5(3)
		C(30)-C(29)-Sb(1)	120.6(4)
		C(34)-C(29)-Sb(1)	120.2(4)
		C(36)-C(35)-Sb(1)	119.3(4)
		C(40)-C(35)-Sb(1)	123.2(3)
		C(46)-C(41)-Sb(2)	122.3(4)
		C(42)-C(41)-Sb(2)	117.8(4)
		C(48)-C(47)-Sb(2)	117.8(4)
		C(52)-C(47)-Sb(2)	119.8(4)
		C(58)-C(53)-Sb(2)	118.6(4)
		C(54)-C(53)-Sb(2)	120.0(4)
		C(64)-C(59)-Sb(2)	122.4(4)
		C(60)-C(59)-Sb(2)	118.9(4)

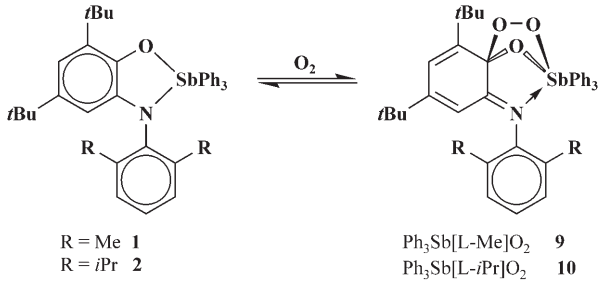

Scheme 3.

700–1600 cm^{-1}. According to IR spectroscopic data the complexes have ν(O–O) bands in the range of 850–950 cm^{-1}.[12] Formation of **11** and **12** is also evident from changes in the electronic absorption spectra. Electronic absorption spectra of **11** and **12** exhibit the appearance of new bands (λ_{max} = 383 and 372 nm, respectively), while the intensity of absorption bands at λ_{max} = 295 nm for **3** and λ_{max} = 299 nm for **5** decrease.

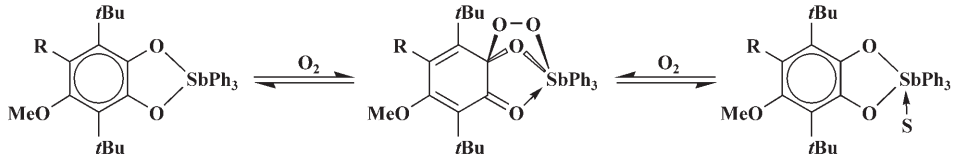

Scheme 4.

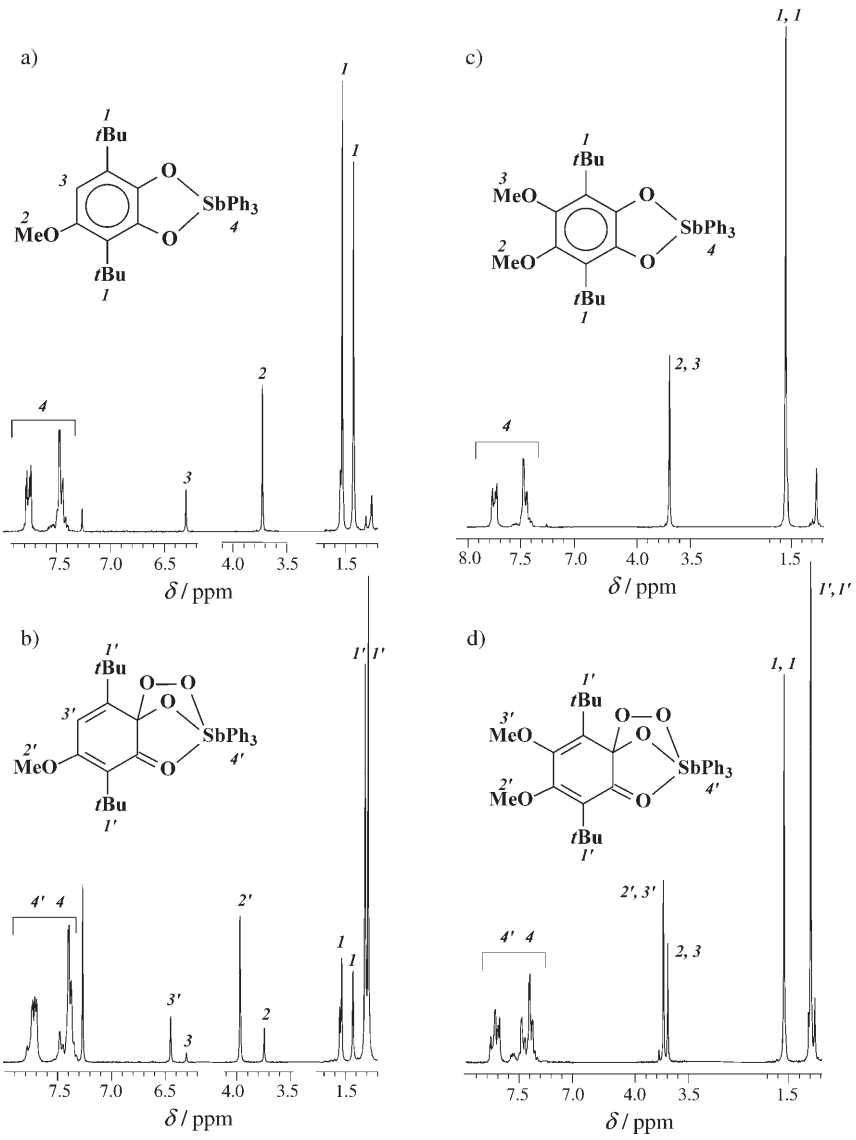

Figure 4. ^{1}H NMR spectra of **3** (a) and **5** (c) and their dioxygen adducts **11** (b) and **12** (d) in $CDCl_3$ at ambient temperature. ^{1}H NMR spectra b) and d) contain residual signals of the initial complexes.

Crystal structures of 9–13: Spiroendoperoxides **9**, **10**, and **12** were isolated from acetone, **11** from toluene and **13** from CH_2Cl_2/hexane as air-stable yellow-orange crystals. Complex **10** contains one molecule of acetone of solvation per molecule of complex. The crystal structures of **9–13** were determined by single-crystal X-ray diffraction. Molecular structures of **9** and **11–13** are depicted in Figures 5–8. Crystallographic data and details of structure determination are given in Table 5. Tables 6–9 summarize selected bond lengths and angles.

All spiroendoperoxide complexes **9–13** have the same structure of five-atom dioxaazastibolane (for **9**, **10**) or trioxastibolane (for **11–13**) rings. The Sb atoms in **9–13** have a distorted octahedral geometry. Atoms O(1) and N(1) in **9**, **10** as well as oxygen atoms O(1), O(2) in **11–13** and two phenyl groups are in equatorial planes, whereas the peroxo atoms O(3) of **9–13** and the third phenyl group are in axial positions.

The molecular structure of spiroendoperoxide **10** was described earlier.[4] In contrast to **10** with isopropyl-substituted *N*-aryl fragment, complex **9** has less bulky methyl groups at *N*-aryl. The most significant difference between these complexes is in the Sb(1)···N(1) distances. Unexpectedly the Sb(1)···N(1) distance in **9** (2.480(1) Å) is significantly longer than that in **10** (2.425(3) Å), whereas the Sb(1)–O(1), Sb(1)–O(2), and Sb(1)–C_{Ph} bond lengths in both complexes are approximately equal. Apparently, the significant difference in the Sb(1)···N(1) distances is determined by crystal-packing effects. Note that the shortest intramolecular distances between *N*-aryl substituents and equatorial Ph groups are 3.432(3) Å in **9** and 3.206(3) Å in **10**.

The N(1)–C(6) and N(1)–C(2) distances in **9** and **10** are 1.291(2) and 1.287(4) Å, respectively, and are typical for N=C bonds.[13] The O(2)–O(3) distances in the peroxide fragments are 1.461(3) Å in **10** and 1.466(2) Å in **9**, which are close to the O–O distances in the antimony endoperoxide 3,3-dihydro-5,5-dimethyl-3,3,3-triphenyl-1,2,4,3-trioxastibolane (1.468 Å)[14] and tetrakis(diaryl-

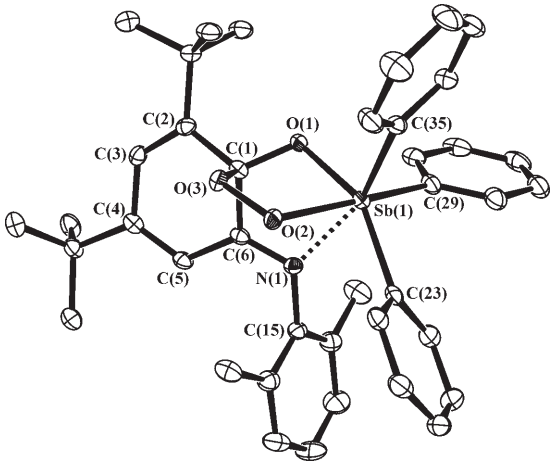

Figure 5. An ORTEP view of **9** with 50% probability ellipsoids (H atoms are omitted).

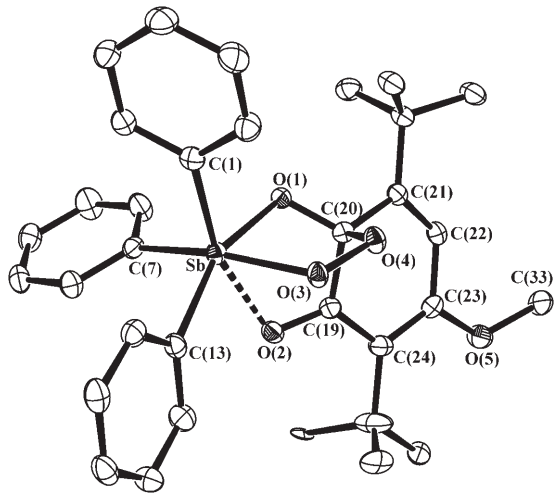

Figure 6. An ORTEP view of **11** with 50% probability ellipsoids (H atoms omitted).

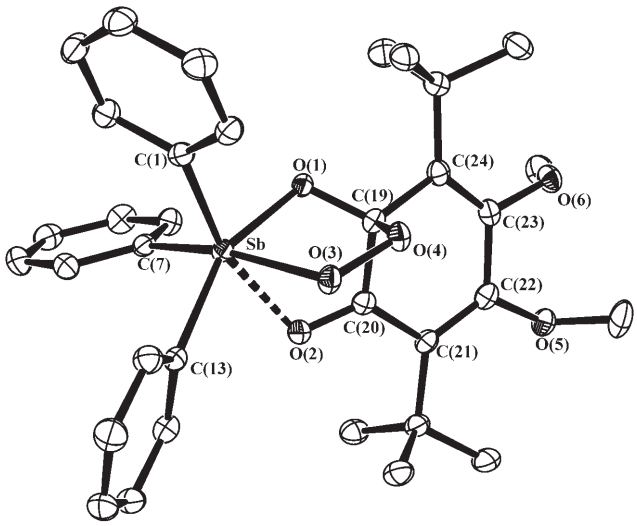

Figure 7. An ORTEP view of **12** with 50% probability ellipsoids (H atoms omitted).

antimony)di-μ_4-peroxotetraoxides $(Ph_2SbO)_4(O_2)_2$ (1.47 Å).[15] Since the C(1) atoms in **9** and **10** have sp^3 hybridization, the Sb(1)-O(1)-N(1)-C(1)-C(6) (**9**) and Sb(1)-O(1)-N(1)-C(1)-C(2) metallocycles (**10**) of the *o*-amidophenolato ligands are not planar.

The bond lengths in the six-membered C(1–6) fragments of **9** and **10** are redistributed relative to the initial *o*-amidophenolate complexes. In **9**, the C(1)–C(2) (1.522(2) Å),

Table 5. Summary of crystal and refinement data for **9**, **11**, **12**, and **13**.

	Ph_3Sb[L-Me]O_2 (**9**)	Ph_3Sb[(MeO)L′]O_2 (**11**)	Ph_3Sb[$(MeO)_2$L′]O_2 (**12**)	Ph_3Sb[PhenL′]O_2 (**13**)
empirical formula	$C_{40}H_{44}NO_3Sb$	$C_{40}H_{45}O_5Sb$	$C_{34}H_{39}O_6Sb$	$C_{32}H_{23}O_4Sb$
formula weight	708.51	727.51	665.40	593.25
temperature [K]	100(2)	100(2)	100(2)	100(2)
wavelength [Å]	0.71073	0.71073	0.71073	0.71073
crystal system	triclinic	monoclinic	monoclinic	triclinic
space group	$P\bar{1}$	$P2(1)/c$	$P2(1)/c$	$P\bar{1}$
a [Å]	10.6939(6)	11.3086(9)	18.3155(9)	9.2366(10)
b [Å]	12.1357(6)	31.344(3)	15.2211(8)	9.3098(11)
c [Å]	15.2329(8)	11.1688(9)	11.6209(6)	14.2320(17)
α [°]	99.5940(10)	90	90	88.034(3)
β [°]	107.7280(10)	117.5480(10)	108.2460(10)	83.994(3)
γ [°]	106.6190(10)	90	90	83.217(3)
V [Å^3]	1733.22(16)	3510.0(5)	3076.8(3)	1208.3(2)
Z	2	4	4	2
ρ_{calcd} [Mg m^{-3}]	1.358	1.377	1.436	1.631
absorption coefficient [mm^{-1}]	0.834	0.829	0.940	1.181
crystal size [mm]	0.35×0.18×0.10	0.15×0.10×0.08	0.35×0.20×0.15	0.08×0.07×0.06
reflections collected	9592	27556	23897	6185
independent reflections	6079 [R(int) = 0.0201]	6183 [R(int) = 0.0215]	5413 [R(int) = 0.0199]	3778 [R(int) = 0.0323]
absorption correction	SADABS	SADABS	SADABS	SADABS
max./min. transmission	0.9213/0.7590	0.9367/0.8858	0.8719/0.7344	0.9325/0.9115
refinement method	full-matrix least-squares on F^2	full-matrix least-squares on F^2	full-matrix least-squares on F^2	full-matrix least-squares on F^2
data/restraints/parameters	6079/0/582	6183/12/574	5413/0/526	3778/0/426
final R indices[a] [$I > 2\sigma(I)$]				
$R1$	0.0273	0.0309	0.0188	0.0392
$wR2$	0.0626	0.0713	0.0478	0.0921
R indices[a] (all data)				
$R1$	0.0330	0.0337	0.0199	0.0487
$wR2$	0.0642	0.0726	0.0485	0.0955
GOF[b] on F^2	1.05	1.088	1.059	1.008
largest diff. peak/hole [e Å^{-3}]	0.768/−0.33	1.199/−1.240	0.567/−0.321	1.274/−0.926

[a] $R = \Sigma||F_o| - |F_c||/\Sigma|F_o|$; $wR = R(wF^2) = [\Sigma w(F_o^2 - F_c^2)^2/\Sigma w(F_o^2)^2]^{1/2}$, $w = 1/[\sigma^2(F_o^2) + (aP)^2 + bP]$, $P = [2F_c^2 + F_o^2]/3$. [b] $GOF = [\Sigma w(F_o^2 - F_c^2)^2/(n-p)]^{1/2}$, where n is the number of reflections, and p the number of refined parameters.

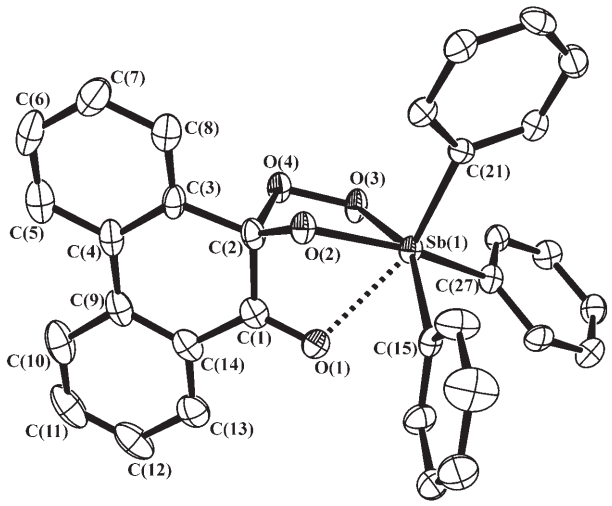

Figure 8. An ORTEP view of **13** with 50% probability ellipsoids (H atoms omitted).

Table 6. Selected bond lengths [Å] and angles [°] for $Ph_3Sb[L\text{-}Me]O_2$ (**9**).

Sb(1)−O(1)	2.0240(10)	O(1)-Sb(1)-O(2)	79.87(4)
Sb(1)−O(2)	2.0731(11)	O(1)-Sb(1)-C(35)	97.53(5)
Sb(1)−C(35)	2.1374(17)	O(2)-Sb(1)-C(35)	93.07(5)
Sb(1)−C(23)	2.1378(16)	O(1)-Sb(1)-C(23)	153.13(6)
Sb(1)−C(29)	2.1441(16)	O(2)-Sb(1)-C(23)	84.87(5)
Sb(1)−N(1)	2.4802(14)	C(35)-Sb(1)-C(23)	105.30(6)
O(1)−C(1)	1.3703(19)	O(1)-Sb(1)-C(29)	89.79(5)
O(2)−O(3)	1.4659(15)	O(2)-Sb(1)-C(29)	165.66(5)
O(3)−C(1)	1.4675(17)	C(35)-Sb(1)-C(29)	98.15(6)
N(1)−C(6)	1.291(2)	C(23)-Sb(1)-C(29)	100.63(6)
N(1)−C(15)	1.443(2)	O(1)-Sb(1)-N(1)	70.22(4)
C(1)−C(2)	1.522(2)	O(2)-Sb(1)-N(1)	73.97(4)
C(1)−C(6)	1.527(2)	C(35)-Sb(1)-N(1)	163.28(6)
		C(23)-Sb(1)-N(1)	84.40(5)
		C(29)-Sb(1)-N(1)	93.26(6)
		C(1)-O(1)-Sb(1)	108.00(8)
		O(3)-O(2)-Sb(1)	110.55(6)
		O(2)-O(3)-C(1)	106.75(10)
		C(6)-N(1)-C(15)	120.02(14)
		C(6)-N(1)-Sb(1)	105.11(11)
		C(15)-N(1)-Sb(1)	131.60(10)
		O(1)-C(1)-O(3)	109.37(12)
		O(1)-C(1)-C(2)	114.64(12)
		O(3)-C(1)-C(2)	102.83(12)
		O(1)-C(1)-C(6)	110.29(14)
		O(3)-C(1)-C(6)	104.48(11)
		C(2)-C(1)-C(6)	114.35(14)

C(1)−C(6) (1.527(2) Å) and C(4)−C(3) (1.477(2) Å) distances correspond to single bonds, whereas C(2)−C(3) (1.334(2) Å) and C(4)−C(5) (1.338(2) Å) are double bonds.[13] The C(5)−C(6) (1.435(2) Å) distance indicates conjugation in the N(1)=C(6)−C(5) fragment. The same is observed in **10**.

Despite their similar nature, complexes **11** and **12** have an unexpected difference in the Sb(1)···O(2) bond lengths. The Sb(1)···O(2) distances are 2.311(2) and 2.4074(9) Å for **11** and **12**, respectively. At the same time other Sb−O distances are close to each other: Sb(1)−O(1) 2.033(2), Sb(1)−O(3) 2.076(1) Å in **11** and Sb(1)−O(1) 2.038(1), Sb(1)−O(3) 2.067(1) Å in **12**. The O(2)−C(19) distance in **11** and O(2)−C(20) distance in **12** are 1.256(3) Å and 1.238(2) Å, respectively, and differ from each other less significantly than the

Table 7. Selected bond lengths [Å] and angles [°] for $Ph_3Sb[(MeO)L']O_2$ (**11**).

Sb(1)−O(1)	2.0334(15)	O(1)-Sb(1)-O(3)	79.86(6)
Sb(1)−O(3)	2.0759(14)	O(1)-Sb(1)-C(1)	93.38(7)
Sb(1)−C(1)	2.130(2)	O(3)-Sb(1)-C(1)	94.17(7)
Sb(1)−C(13)	2.142(2)	O(1)-Sb(1)-C(13)	158.57(7)
Sb(1)−C(7)	2.143(2)	O(3)-Sb(1)-C(13)	85.66(7)
Sb(1)−O(2)	2.3112(15)	C(1)-Sb(1)-C(13)	103.42(8)
O(1)−C(20)	1.364(3)	O(1)-Sb(1)-C(7)	91.47(7)
C(1)-C(2)	1.391(3)	O(3)-Sb(1)-C(7)	162.98(7)
C(1)−C(6)	1.394(3)	C(1)-Sb(1)-C(7)	101.00(8)
O(2)−C(19)	1.256(3)	C(13)-Sb(1)-C(7)	98.15(8)
O(3)−O(4)	1.475(2)	O(1)-Sb(1)-O(2)	72.24(6)
O(4)−C(20)	1.472(3)	O(3)-Sb(1)-O(2)	74.40(5)
O(5)−C(23)	1.339(3)	C(1)-Sb(1)-O(2)	162.79(7)
O(5)−C(33)	1.447(3)	C(13)-Sb(1)-O(2)	88.75(7)
C(19)−C(20)	1.542(3)	C(7)-Sb(1)-O(2)	89.04(7)
C(20)−C(21)	1.499(3)	C(20)-O(1)-Sb(1)	107.09(13)
		C(2)-C(1)-C(6)	118.8(2)
		C(2)-C(1)-Sb(1)	121.24(14)
		C(6)-C(1)-Sb(1)	119.87(17)
		C(19)-O(2)-Sb(1)	109.51(13)
		C(3)-C(2)-C(1)	120.6(2)
		O(4)-O(3)-Sb(1)	110.17(10)
		C(4)-C(3)-C(2)	120.0(2)
		O(1)-C(20)-O(4)	109.16(16)
		O(1)-C(20)-C(21)	114.29(19)
		O(4)-C(20)-C(21)	104.47(16)
		O(1)-C(20)-C(19)	109.02(17)
		O(4)-C(20)-C(19)	103.00(17)
		C(21)-C(20)-C(19)	116.00(18)

Table 8. Selected bond lengths [Å] and angles [°] for $Ph_3Sb[(MeO)_2L']O_2$ (**12**).

Sb(1)−O(1)	2.0377(10)	O(1)-Sb(1)-O(3)	79.62(4)
Sb(1)−O(3)	2.0667(10)	O(1)-Sb(1)-C(1)	96.53(4)
Sb(1)−C(1)	2.1230(13)	O(3)-Sb(1)-C(1)	96.46(5)
Sb(1)−C(7)	2.1307(15)	O(1)-Sb(1)-C(7)	91.07(4)
Sb(1)−C(13)	2.1322(13)	O(3)-Sb(1)-C(7)	158.51(5)
Sb(1)−O(2)	2.4074(9)	C(1)-Sb(1)-C(7)	103.86(5)
O(1)−C(19)	1.3682(16)	O(1)-Sb(1)-C(13)	155.97(4)
O(2)−C(20)	1.2389(17)	O(3)-Sb(1)-C(13)	83.53(5)
O(3)−O(4)	1.4729(13)	C(1)-Sb(1)-C(13)	102.31(5)
O(4)−C(19)	1.4641(17)	C(7)-Sb(1)-C(13)	98.66(5)
O(5)−C(22)	1.3508(16)	O(1)-Sb(1)-O(2)	69.89(3)
O(5)−C(33)	1.447(2)	O(3)-Sb(1)-O(2)	73.28(4)
O(6)−C(23)	1.3760(17)	C(1)-Sb(1)-O(2)	163.98(4)
O(6)−C(34)	1.4286(19)	C(7)-Sb(1)-O(2)	85.36(4)
C(19)−C(24)	1.5093(18)	C(13)-Sb(1)-O(2)	88.95(4)
C(19)−C(20)	1.5475(18)	C(19)-O(1)-Sb(1)	108.15(8)
		C(2)-C(1)-C(6)	119.19(13)
		C(2)-C(1)-Sb(1)	121.48(10)
		C(6)-C(1)-Sb(1)	119.27(10)
		C(20)-O(2)-Sb(1)	108.25(8)
		C(3)-C(2)-C(1)	120.27(14)
		O(4)-O(3)-Sb(1)	111.31(7)
		O(1)-C(19)-O(4)	110.12(10)
		O(1)-C(19)-C(24)	113.96(11)
		O(4)-C(19)-C(24)	104.31(11)
		O(1)-C(19)-C(20)	107.70(11)
		O(4)-C(19)-C(20)	103.58(10)
		C(24)-C(19)-C(20)	116.53(11)

Table 9. Selected bond lengths [Å] and angles [°] for $Ph_3Sb[PhenL']O_2$ (**13**).

Sb(1)−O(2)	2.044(3)	O(2)-Sb(1)-O(3)	78.78(11)
Sb(1)−O(3)	2.070(3)	O(2)-Sb(1)-C(21)	92.35(15)
Sb(1)−C(21)	2.113(4)	O(3)-Sb(1)-C(21)	104.46(15)
Sb(1)−C(27)	2.135(4)	O(2)-Sb(1)-C(27)	158.60(15)
Sb(1)−C(15)	2.135(4)	O(3)-Sb(1)-C(27)	83.45(14)
Sb(1)−O(1)	2.549(3)	C(21)-Sb(1)-C(27)	103.63(17)
O(1)−C(1)	1.235(6)	O(2)-Sb(1)-C(15)	90.21(14)
C(1)−C(2)	1.517(7)	O(3)-Sb(1)-C(15)	152.22(16)
O(2)−C(2)	1.354(5)	C(21)-Sb(1)-C(15)	101.38(17)
C(2)−O(4)	1.471(5)	C(27)-Sb(1)-C(15)	100.29(17)
O(3)−O(4)	1.461(4)	O(2)-Sb(1)-O(1)	69.50(11)
C(3)−C(4)	1.370(8)	O(3)-Sb(1)-O(1)	70.92(11)
C(3)−C(8)	1.395(7)	C(21)-Sb(1)-O(1)	161.73(14)
C(4)−C(5)	1.372(8)	C(27)-Sb(1)-O(1)	93.52(14)
C(5)−C(6)	1.377(9)	C(15)-Sb(1)-O(1)	81.35(14)
C(6)−C(7)	1.364(9)	C(1)-O(1)-Sb(1)	105.1(3)
C(7)−C(8)	1.405(7)	O(1)-C(1)-C(14)	122.7(5)
C(8)−C(9)	1.463(8)	O(1)-C(1)-C(2)	116.1(4)
C(9)−C(14)	1.411(7)	C(14)-C(1)-C(2)	121.1(4)
C(9)−C(10)	1.416(8)	C(2)-O(2)-Sb(1)	108.8(3)
C(10)−C(11)	1.364(9)	O(2)-C(2)-O(4)	109.4(3)
C(11)−C(12)	1.370(9)	O(2)-C(2)-C(3)	114.0(4)
C(12)−C(13)	1.368(8)	O(4)-C(2)-C(3)	102.4(3)
C(13)−C(14)	1.387(8)	O(2)-C(2)-C(1)	110.3(4)
		O(4)-C(2)-C(1)	104.8(4)
		C(3)-C(2)-C(1)	115.0(4)

Sb(1)···O(2) bond lengths. The C(19)−C(2) bond in **11** and C(20)−C(2) bond in **12** are close to C=O bonds (1.19–1.25 Å).[13] The torsion angles O(1)-C(20)-C(19)-O(2) in **11** and O(1)-C(19)-C(20)-O(2) in **12** are also similar (−30.3 and −30.8°, respectively).

Apparently, the crystal-packing energy in **11** and **12** plays a significant role in the formation of the donor–acceptor Sb···O bonds, as in **9** and **10**.

The C(20)−C(1) (1.364(3) Å) distance in **11** and C(19)−C(1) (1.368(2) Å) distance in **12** are in the range characteristic for catecholate bond lengths (1.35–1.38 Å[6,9,10]) and close to the respective analogous distances in **9** and in **10**. (1.370(2), 1.369(4) Å) $C(sp^3)$−O(4) bond lengths (1.472(3) Å for **11** and 1.464(2) Å for **12**) are in the range of ordinary C−O bond lengths (1.41–1.47 Å),[13] as in **9** (C(1)−O(3) 1.468(2) Å) and **10** (C(1)−O(3) 1.479(4) Å). The peroxide O(3)−O(4) distances of 1.475(2) Å in **11** and 1.464(2) Å in **12** are close to corresponding bonds in known peroxides (1.469 Å).[16]

The nonplanar six-membered C(19–24) rings of complexes **11** and **12** exhibit C−C bond differentiation. The spiro carbon atoms form normal bonds (1.502–1.520 Å).[13] The C(21)−C(22) and C(23)−C(24) bonds (1.336(3) and 1.373(3) Å in **11**, 1.361(2) and 1.342(2) Å in **12**) are close to C=C bonds (1.332 Å).[13] The C(19)−C(24) bond length in **11** is 1.428(3) Å, and the C(20)−C(21) distance in **12** is 1.452(2) Å, which corresponds to conjugated C−C bonds of sp^2 C atoms (1.455 Å).[13]

Interestingly, **11** and **12** have different C(22)−C(23) bond lengths (1.460(3) Å and 1.502(2) Å respectively), possibly due to the influence of methoxyl groups. Complex **11** probably has C(21–24) conjugation; hence, the C(22)−C(23) bond length of 1.460(3) Å in **11** is much shorter than the corresponding bond length in **12** (1.502(2) Å). Moreover, C(21)−C(22) and C(23)−C(24) bond lengths in **11** are longer than those in **12**.

In **13** (Figure 8) the Sb(1)···O(1) (2.549(3) Å) distance has a maximum value in comparison with the analogous distances in **9**–**12**. The O(3)−O(4) bond length in **13** of 1.461(4) Å is shorter than the analogous distance (1.493(5) Å) in a similar Rh complex[17] and somewhat less than in organic endoperoxides (1.48–1.49 Å).[18] The aromaticity of the C(1)-C(2)-C(3)-C(8)-C(9)-C(14) ring is lost because C(2) has sp^3 hybridization. All bond lengths formed with this carbon atom are in the range of normal bonds (C−C 1.515(6)–1.517(7) and C−O 1.354(5)–1.471(5) Å).[13]

Thus, coordination of the oxygen molecule to the initial *o*-amidophenolate and catecholate complexes of Sb(v) leads to:

1) Breaking of the Sb−O (in catecholates) or Sb−N (in *o*-amidophenolates) bond and formation of peroxide Sb−O and C−O bonds in an Sb-O-O-C fragment. As a result, one carbon atom of the catecholate fragment changes its hybridization from sp^2 to sp^3, and the aromaticity of the six-membered C−C ring is lost.
2) Formation of an N=C or C=O bond and donor–acceptor Sb···O or Sb···N bond which vary over wide ranges of values, whereas other geometrical parameters in the coordination spheres of Sb atoms are similar to each other.

Thus, a mechanism of reversible dioxygen binding by **1**–**7** can be suggested (Scheme 5). The first step is one-electron oxidation of *o*-amidophenolato or catecholato ligand by mo-

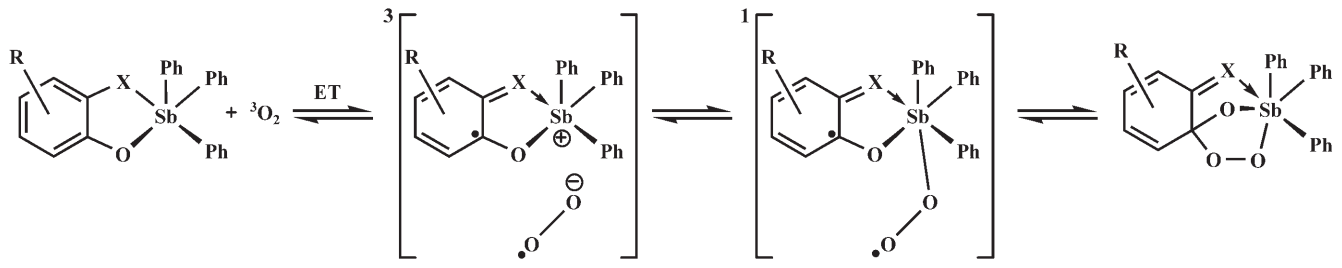

Scheme 5.

lecular oxygen, with intermediate formation of an ion pair consisting of molecular cation and superoxide anion. In the next stage geminate recombination of ion pairs leads to a triplet biradical complex of antimony(v) containing *o*-iminobenzosemiquinonato (or *o*-benzosemiquinonato) and peroxo ligands. Interspin conversion of triplet to singlet state in this radical pair is facilitated by the presence of the heavy antimony atom with a large constant of spin–orbital interaction. The subsequent recombination of the radical centers in this singlet intermediate results in the final bicyclic endoperoxides. The formation of endoperoxide does not take place if the redox conversion from dianionic form (catecholate) to radical anion (*o*-semiquinolate) does not compensate for the energy loss of dioxygen reduction to the radical anion. For example, catecholates of Ph_3Sb(v) with 3,6-di-*tert*-butyl-*o*-benzoquinone or perchloroxanthrene-2,3-quinone are stable towards dioxygen, both in the solid state and in solution.[6] However, the use of electron-donor methoxyl groups (complexes **3**--**6**) to facilitate oxidation of the catecholate ligand or using the easily oxidized phenanthrene-9,10-diolate ligand (**7**) allow dioxygen-binding ability to be achieved. Thus, the redox potential of the ligand in antimony(v) catecholates and *o*-amidophenolates plays a crucial role in the ability of the complex to bind and release O_2.

Experimental Section

General aspects: Starting materials were commercially available (Aldrich, Fluka, Strem) unless otherwise noted. Triphenylantimony was prepared as described in the literature.[19] 4,6-Di-*tert*-butyl-*N*-(2,6-diisopropylphenyl)-*o*-iminobenzoquinone, 4,6-di-*tert*-butyl-*N*-(2,6-di-methylphenyl)-*o*-iminobenzoquinone, 4-methoxy-3,6-di-*tert*-butyl-*o*-benzoquinone and 4,5-di-methoxy-3,6-di-*tert*-butyl-*o*-benzoquinone were prepared according to literature procedures.[20,21] Solvents were purified by standard methods.[22] Syntheses of complexes **1**–**8** were carried out in vacuum.

^{1}H NMR spectra were recorded on Bruker AVANCE DPX-200 spectrometer in $CDCl_3$ or [D_6]acetone and with TMS as internal standard. IR spectra were recorded on a Specord M-80. Electronic absorption spectra were recorded on a Perkin-Elmer Lambda 25 UV/Vis spectrometer (range: 220–1100 nm) at ambient temperature. X-ray structure analysis was carried out on a Smart Apex diffractometer (Bruker AXS).

[4,6-Di-*tert*-butyl-*N*-(2,6-dimethylphenyl)-o-amidophenolato]triphenylantimony(v) (Ph_3Sb[AP-Me], 1): Triphenylantimony (0.353 g, 1 mmol) was dissolved in dry toluene (20 mL). 4,6-Di-*tert*-butyl-*N*-(2,6-dimethylphenyl)-*o*-iminobenzoquinone (0.676 g, 1 mmol) dissolved in toluene (30 mL) was added dropwise to the triphenylantimony solution over 10 min. The red-brown solution of free *o*-iminobenzoquinone IBQ-Me lightened as each drop came into contact and reacted with the triphenylantimony solution. After addition was complete, the reaction mixture became yellow. Removal of solvent under vacuum yielded a solid. Recrystallization of this crude material from hexane yielded yellow microcrystalline product; m.p. 167–168 °C. Yield 0.99 g (96 %). Elemental analysis calcd (%) for $C_{40}H_{44}ONSb$: C 71.01, H 6.51, Sb 18.05; found: C 71.36, H 6.22, Sb 17.84; IR (Nujol): $\tilde{\nu}$ = 1570m, 1510w, 1450s, 1440s, 1420s, 1385s, 1365m, 1335m, 1305w, 1295m, 1255s, 1245s, 1205w, 1185w, 1165w, 1120w, 1095w, 1070m, 1025m, 995s, 920w, 895m, 855m, 830m, 765m, 760w, 725s, 695s, 675w, 655w, 605w, 545w, 530w, 515w, 490w, 450m cm^{-1}; ^{1}H NMR (200 MHz, $CDCl_3$, 25 °C, TMS): δ = 1.15 and 1.49 (both s, both 9H; 2*t*Bu), 1.98 (s, 6H; 2Me), 5.87 and 6.75 (d, both 1H; ^4J(H,H) = 2.3, C_6H_2 aromatic), 6.69 (s, 3H; C_6H_3 aromatic), 7.21–7.55 ppm (m, 15H; aromatic); ^{1}H NMR (200 MHz, [D_6]acetone, 25 °C, TMS): δ = 1.11 and 1.46 (both s, both 9H; 2*t*Bu), 1.99 (s, 6H; 2Me), 5.86 and 6.73 (d, both 1H; ^4J(H,H) = 2.3, C_6H_2 aromatic), 6.75 (s, 3H; C_6H_3 aromatic), 7.32–7.57 ppm (m, 15H; aromatic).

[4,6-Di-*tert*-butyl-*N*-(2,6-diisopropylphenyl)-*o*-amidophenolato]triphenylantimony(v) (Ph_3Sb[AP-iPr], 2): This complex was prepared as described previously.[4]

(4-Methoxy-3,6-di-*tert*-butylcatecholato)triphenylantimony(v) Ph_3Sb[(MeO)Cat] (3): Synthesis and isolation of **3** were carried out similarly to those of **2**. Thus, the reaction of triphenylantimony (0.353 g, 1 mmol) and 4-methoxy-3,6-di-*tert*-butyl-*o*-benzoquinone (0.250 g, 1 mmol) yielded **3** (0.585 g; 97 %) as yellow crystals; m.p. 104–105 °C. Elemental analysis calcd (%) for $C_{33}H_{37}O_3Sb$: C 65.67, H 6.45, Sb 20.23; found: C 65.23, H 6.83, Sb 20.05; IR (Nujol): $\tilde{\nu}$ = 1596w, 1548w, 1477s, 1434s, 1393s, 1378s, 1356w, 1329w, 1305w, 1258w, 1238s, 1198m, 1095s, 1075m, 1063w, 1022w, 988m, 977m, 929w, 886s, 849w, 816m, 794w, 742s, 732s, 692s, 672w, 618w, 587w, 549w, 485m, 455s cm^{-1}; ^{1}H NMR (200 MHz, $CDCl_3$, 25 °C, TMS): δ = 1.44–1.56 (both s, both 9H; 2*t*Bu), 3.74 (s, 3H, OMe), 6.33 (s, 1H, C_6H_1), 7.38–7.79 ppm (m, 15H, aromatic).

(4,5-Dimethoxy-3,6-di-*tert*-butylcatecholato)triphenylantimony(v) methanolate, 3·CH_3OH (4): Synthesis and isolation of **4** were carried out similarly to those of **3**. Compound **3** was recrystallized from methanol to give yellow microcrystals of **4**; m.p. 110–111 °C. Elemental analysis calcd (%) for $C_{36}H_{49}O_6Sb$: C 61.76, H 7.01, Sb 17.44; found: C 62.22, H 7.33, Sb 17.03; IR (Nujol): $\tilde{\nu}$ = 3420m, 1600w, 1555w, 1495s, 1435s, 1385s, 1360m, 1340s, 1310w, 1265w, 1295s, 1245s, 1240s, 1200m, 1100s, 1075m, 1035w, 1025m, 995m., 820m, 795w, 735s, 695s, 665w, 620w, 585w, 545w, 485m, 455m cm^{-1}; ^{1}HNMR (200 MHz, $CDCl_3$, 25 °C, TMS): δ = 1.42 and 1.53 (both s, both 9H; 2*t*Bu), 3.48 (s, 3H, CH_3OH), 3.72 (s, 3H, OMe), 6.30 (s, 1H, C_6H_1), 7.37–7.78 ppm (m, 15H, aromatic).

(4,5-Dimethoxy-3,6-di-*tert*-butylcatecholato)triphenylantimony(v) (Ph_3Sb[$(MeO)_2$Cat], 5): Synthesis and isolation were carried out similarly to those of **2**. Thus, the reaction of triphenylantimony (0.353 g, 1 mmol) and 4,5-di-methoxy-3,6-di-*tert*-butyl-*o*-benzoquinone (0.280 g, 1 mmol) yielded **5** (0.608 g; 96 %) as yellow crystals; m.p. 141–142 °C. Elemental analysis calcd (%) for $C_{34}H_{39}O_4Sb$: C 64.47, H 6.21, Sb 19.27; found: C 64.19, H 6.23, Sb 18.79; IR (Nujol): $\tilde{\nu}$ = 1478m, 1435s, 1382s, 1356m, 1334w, 1301w, 1272m, 1222m, 1202w, 1191w, 1180w, 1102m, 1058s, 1022m, 993s, 928w, 904s, 885m, 849w, 796w, 776w, 734s, 693s, 657w, 634m, 584s, 547w, 508w, 463m, 448s cm^{-1}. ^{1}H NMR (200 MHz, $CDCl_3$, 25 °C, TMS): δ = 1.54 (s, 9H; 2*t*Bu), 3.69 (s, 6H, 2OMe), 7.38–7.77 ppm (m, 15H, aromatic).

3,6-Di-*tert*-butyl-4,5-dimethoxycatecholato)triphenylantimony(v) acetonitrile solvate, 5·CH_3CN (6): Synthesis and isolation of **6** were carried out similarly to those of **5**. Compound **5** was recrystallized from acetonitrile to give yellow microcrystals of **6**; m.p. 105–106 °C. Elemental analysis calcd (%) for $C_{36}H_{42}NO_4Sb$: C 64.05, H 6.23, Sb 18.09; found: C 64.49, H 6.56, Sb 18.53; IR (Nujol): $\tilde{\nu}$ = 2290w, 2259w, 1596w, 1546w, 1476m, 1435s, 1355m, 1335w, 1304w, 1273m, 1226m, 1196m, 1181w, 1155w, 1109m, 1059s, 1022w, 996m, 979m, 911m, 880m, 774w, 732s, 694s, 659w, 631w, 581w, 548w, 520w, 455s cm^{-1}; ^{1}H NMR (200 MHz, $CDCl_3$, 25 °C, TMS): δ = 1.31 (s, 9H; 2*t*Bu), 1.57 (s, 6H, 2CH_3CN), 3.75 (s, 6H, 2OMe), 7.33–7.74 ppm (m, 15H, aromatic).

Ph_3Sb[PhenCat] (7): Synthesis and isolation of **7** were carried out similarly to those of **2**. Thus, the reaction of triphenylantimony (0.353 g, 1 mmol) and 9,10-phenanthrenequinone (0.208 g, 1 mmol) yielded **7** (0.451 g; 80.4 %) as air-unstable green crystals. Elemental analysis calcd (%) for $C_{32}H_{23}O_2Sb$: C 68.45, H 4.1, Sb 21.75; found: C 68.83, H 4.63, Sb 21.99; IR (Nujol): $\tilde{\nu}$ = 1605w, 1585m, 1570w, 1525w, 1495m, 1380s, 1355m, 1340m, 1295s, 1255s, 1255m, 1185w, 1155w, 1120m, 1095w, 1065s, 1035w, 1025s, 995w, 945w, 925w, 800w, 785m, 750s, 740s, 715s, 695s, 690s, 675w, 660w, 555w, 545w, 510m, 455m cm^{-1}.

[Ph_4Sb]$^+$[Ph_2Sb(PhenCat)$_2$]$^-$ (8): Synthesis and isolation of **8** were carried out similarly to those of **2**. Thus, the reaction of triphenylantimony (0.353 g, 1 mmol) and 9,10-phenanthrenequinone (0.208 g, 1 mmol) yielded **8** (0.521 g; 93 %) as a yellow solid. Recrystallization of this crude material from CH_2Cl_2/hexane yielded yellow microcrystalline product; m.p. 140–141 °C (decomp). Elemental analysis calcd (%) for $C_{65}H_{48}Cl_2O_4Sb_2$: C 64.60, H 3.98, Sb 20.20; found: C 65.03, H 3.63, Sb 20.05; IR (Nujol):

$\tilde{\nu}$ = 1600w, 1580m, 1514w, 1490w, 1440s, 1416m, 1373s, 1341s, 1307w, 1283w, 1264w, 1225w, 1172w, 1108m, 1069w, 1055m, 1026m, 996w, 938m, 792m, 757s, 733s, 730s, 723s, 697w, 686m, 629w, 598w, 587w, 574w, 550w, 509w, 455m, 442m cm^{-1}.

$Ph_3Sb[L\text{-}Me]O_2$ (9): The synthesis of **9** was carried out similarly to that of **10** described in reference [4]. Compound **1** (100 mg, 0.148 mmol) was dissolved in toluene in air. The solution was allowed to stand for 2 h. Then solvent was removed by slow evaporation, and the residue recrystallized from acetone over three days to yellow-orange crystals of **9** suitable for X-ray diffraction, which were dried in air. Yield 100.2 mg (96%); m.p. 36–137°C (decomp). IR (Nujol) = $\tilde{\nu}$ = 1720w, 1645m, 1600m, 1595m, 1575s, 1485m, 1465s, 1440s, 1375s, 1365m, 1360w, 1345w, 1310w, 1260w, 1255w, 1220m, 1180s, 1135s, 1095w, 1075m, 1025w, 1000w, 985w, 925w, 910m, 900m, 875w, 855m, 835w, 820w, 800w, 775m, 745s, 735s, 725m, 695s, 660m, 620w, 595w, 555w, 540w, 510w, 470m, 465m, 455m, 450m cm^{-1}; ^{1}H NMR (200 MHz, $CDCl_3$, 25°C, TMS): δ = 1.02 and 1.36 (both s, both 9H; 2*t*Bu), 1.15 (s, 6H; 2Me), 5.42 and 6.47 (d, both 1H, ^4J(H,H) = 1.6; C_6H_2 aromatic), 6.69 (s, 3H; C_6H_3 aromatic), 7.21–7.55 ppm (m, 15H; aromatic); ^{1}H NMR (200 MHz, [D_6]acetone, 25°C, TMS): δ = 1.04 and 1.38 (both s, both 9H; 2*t*Bu), 1.99 (s, 6H; 2Me), 5.5 and 6.65 (d, both 1H, ^4J(H,H) = 1.6; C_6H_2 aromatic), 6.75 (s, 3H; C_6H_3 aromatic), 7.32–7.57 ppm (m, 15H; aromatic).

$Ph_3Sb[(MeO)L']O_2$ (11): Compound **3** or **4** (100mg, 0.145 mmol for **3**, 0.143 mmol for **4**) was dissolved in toluene in air. This solution was allowed to stand for five days to give X-ray-quality yellow-orange crystals of **11**, which were dried in air. Yield 100.5 mg (96%); m.p. 85–87°C (decomp). IR (Nujol): $\tilde{\nu}$ = 1655m, 1610w, 1570w, 1510s, 1480s, 1435s, 1410s, 1395m, 1375m, 1360m, 1345m, 1305m, 1255s, 1235s, 1205m, 1190w, 1175m, 1145m, 1095m, 1075m, 1025m, 1000w, 965s, 955w, 900m, 875m, 810w, 765w, 740s, 730s, 695s, 655w, 615m, 575w, 495w, 460m, 450m cm^{-1}; ^{1}H NMR (200 MHz, $CDCl_3$, 25°C, TMS): δ = 1.28 and 1.31 (s, both 9H; 2*t*Bu), 3.95 (s, 3H; OMe), 6.44 (s, 1H, C_6H_1), 7.37–7.78 ppm (m, 15H; aromatic).

$Ph_3Sb[(MeO)_2L']O_2$ (12): Compound **5** or **6** (100 mg, 0.158 mmol (**5**), 0.148 mmol (**6**)) was dissolved in toluene in air. The solution was allowed to stand for 2 h. Then solvent was removed by slow evaporation, and the residue recrystallized from acetone over three days to give X-ray-suitable yellow-orange crystals of **12**, which were dried in air. Yield 100.1 mg (95%); m.p. 105–107°C (decomp). IR (Nujol): $\tilde{\nu}$ = 1715s, 1610m, 1550s, 1485s, 1445s, 1400w, 1385m, 1345s, 1310w, 1295w, 1275m, 1250m, 1225m, 1205w, 1190w, 1155m, 1110w, 1070m, 1055s, 1015m, 1000w, 975s, 950w, 900w, 890m, 875m, 840w, 810w, 785m, 735s, 730s, 695s, 680w, 670w, 580w, 530w, 515w, 475w, 450m cm^{-1}; ^{1}H NMR (200 MHz, $CDCl_3$, 25°C, TMS): δ = 1.29 (s, 9H; 2 *t*Bu), 3.73 (s, 6H; 2OMe), 7.37–7.76 ppm (m, 15H; aromatic).

$Ph_3Sb[PhenL']O_2$ (13): Compound **7** (100 mg, 0.178 mmol) was dissolved in CH_2Cl_2/hexane and allowed to stand for 3 h to give the X-ray-suitable yellow-orange crystals of **13**, which were dried in air. Yield 102.4 mg (97%); m.p. 108–110°C (decomp). IR (Nujol): ν = 1675w, 1639m, 1593m, 1478m, 1434s, 1334m, 1308m, 1295m, 1282m, 1254w, 1231w, 1181w, 1170w, 1161m, 1109w, 1073m, 1065w, 1050w, 1033w, 1024w, 998m, 949m, 925w, 891w, 851w, 764m, 746s, 738s, 719m, 694s, 664m, 617w, 590w, 566w, 536w, 483m, 457s, 437w cm^{-1}.

X-ray diffraction studies: Suitable crystals for X-ray diffraction were prepared by prolonged crystallization from toluene for **2, 3, 5, 8**, and **11**, methanol for **4**, acetonitrile for **6**, acetone for **9**, **10**, and **12** and CH_2Cl_2/hexane for **13**.

Intensity data were collected on a Smart Apex diffractometer with graphite-monochromated $Mo_{K\alpha}$ radiation (λ = 0.71073 Å) in the ϕ-ω scan mode (ω = 0.3°, 10 s on each frame). Absorption corrections were made by SADABS program.[23] The structures were solved by direct methods and refined on F^2 by full-matrix least-squares techniques using SHELXTL.[24] All non-hydrogen atoms were refined anisotropically. The H atoms in **8** were placed in calculated positions and refined in the riding model (U_{iso}(H) = 1.2 U_{eq}(C) Å^2 for aromatic hydrogen and 1.5 U_{eq}(C) Å^2 for alkyl hydrogen atoms), and those in **4**, **6**, **9**, **12**, and **13** were located by Fourier synthesis and refined isotropically. In **11** some of the hydrogen atoms were placed in calculated positions and refined in the riding model, and the others were located by Fourier synthesis and refined isotropically. Two MeOH solvent molecules in **4**, one CH_2Cl_2 in **8** and one toluene in **11** in common position were found.

Tables 1 and 5 summarize the crystal data and some details of data collection and refinement for **4**, **6**, **8**, **9**, and **11**–**13**. Selected bond lengths and angles for **4**, **6**, **8**, **9**, and **11**–**13** are given in Tables 2–4 and 6–9.CCDC-289294 (**4**), CCDC-289295 (**6**), CCDC-289296 (**8**), CCDC-289297 (**9**), CCDC-289298 (**11**), CCDC-289299 (**12**), and CCDC-289300 (**13**) contain the supplementary crystallographic data for this paper. These data can be obtained free of charge from the Cambridge Crystallographic Data Centre via www.ccdc.cam.ac.uk/data_request/cif.

Acknowledgement

We are grateful to the Russian Foundation for Basic Research (grants 04-03-32409), Russian President Grant supporting scientific schools (grants 1649.2003.3 and 1652.2003.3), and Russian Science Support Foundation (A.I. Poddel'sky) for financial support of this work. Spectroscopic investigations were carried out in the Analytical Centre of IMOC RAS.

[1] a) M. N. Hughes, *The Inorganic Chemistry of Biological Processes*, 2nd ed., Wiley, Chichester, **1981**; b) A. Gelasco, S. Bensiek, V. L. Pecoraro, *Inorg. Chem.* **1998**, *37*, 3301; c) E. I. Solomon, T. C. Brunold, M. I. Davis, J. N. Kemsley, S.-K. Lee, N. Lehnert, F. Neese, A. J. Skulan, Y.-S. Yang, J. Zhou, *Chem. Rev.* **2000**, *100*, 235.

[2] a) J. P. Collman, T. R. Halbert, K. S. Suslick in *Metal Ion Activation of Dioxygen* (Ed.: T. G. Spiro), Wiley, New York, **1980**, chap. I; b) P. M. Harrison, R. J. Hoare, *Metals in Biochemistry*, Chapman and Hall, London, **1980**; c) D. A. Phipps, *Metals and Metabolism*, Oxford University Press, Oxford, **1976**; d) *New Trends in Bioinorganic Chemistry* (Eds.: R. J. P. Williams, J. J. R. F. da Silva), Academic, London, **1978**.

[3] a) J. Almog, J. E. Baldwin, R. L. Dyer, M. Peters, *J. Am. Chem. Soc.* **1975**, *97*, 226; b) J. P. Collman, F. C. Anson, C. E. Barnes, C. S. Bencosme, T. Geiger, E. R. Evitt, R. P. Kreh, K. Meier, R. B. Pettrnan, *J. Am. Chem. Soc.* **1983**, *105*, 2694; c) J. P. Collman, *Acc. Chem. Res.* **1977**, *10*, 265; d) K. S. Suslick, M. M. Fox, *J. Am. Chem. Soc.* **1983**, *105*, 3507.

[4] G. A. Abakumov, A. I. Poddel'sky, E. V. Grunova, V. K. Cherkasov, G. K. Fukin, Yu. A. Kurskii, L. G. Abakumova, *Angew. Chem.* **2005**, *117*, 2827–2831; *Angew. Chem. Int. Ed.* **2005**, *44*, 2767–2771.

[5] a) H. Chun, C. N. Verani, P. Chaudhuri, E. Bothe, E. Bill, T. Weyhermuller, K. Wieghardt, *Inorg. Chem.* **2001**, *40*, 4157–4166; b) H. Chun, P. Chaudhuri, T. Weyhermuller, K. Wieghardt, *Inorg. Chem.* **2002**, *41*, 790–795; c) K. S. Min, T. Weyhermuller, K. Wieghardt, *Dalton Trans.* **2004**, 178–186; d) X. Sun, H. Chun, K. Hildenbrand, E. Bothe, T. Weyhermuller, F. Neese, K. Wieghardt, *Inorg. Chem.* **2002**, *41*, 4295–4303; e) P. Chaudhuri, C. N. Verani, E. Bill, E. Bothe, T. Weyhermuller, K. Wieghardt, *J. Am. Chem. Soc.* **2001**, *123*, 2213–2223; f) D. Herebian, P. Ghosh, H. Chun, E. Bothe, T. Weyhermuller, K. Wieghardt, *Eur. J. Inorg. Chem.* **2002**, 1957–1967; g) P. Chaudhuri, M. Hess, K. Hildenbrand, E. Bill, T. Weyhermuller, K. Wieghardt, *Inorg. Chem.* **1999**, *38*, 2781–2790.

[6] V. K. Cherkasov, E. V. Grunova, A. I. Poddel'sky, G. K. Fukin, Yu. A. Kurskii, L. G. Abakumova, G. A. Abakumov, *J. Organomet. Chem.* **2005**, *690*, 1273–1281.

[7] G. A. Abakumov, V. K. Cherkasov, E. V. Grunova, A. I. Poddel'sky, L. G. Abakumova, Yu. A. Kurskii, G. K. Fukin, E. V. Baranov, *Dokl. Chem.* **2005**, *405*, 119–203.

[8] P. L. Millington, D. B. Sowerby, *J. Chem. Soc. Dalton Trans.* **1992**, 1199–1204.

[9] G. K. Fukin, L. N. Zakharov, G. A. Domrachev, A. U. Fedorov, S. N. Zaburdyaeva, V. A. Dodonov, *Russ. Chem. Bull.* **1999**, *9*, 1744–1753.

[10] a) M. Hall, D. B. Sowerby, *J. Am. Chem. Soc.* **1980**, *102*, 628–632; b) R. R. Holmes, R. O. Day, V. Chandrasekhar, J. M. Holmes, *Inorg.*

Chem. **1987**, *26*, 157–163; c) R. R. Holmes, R. O. Day, V. Chandrasekhar, J. M. Holmes, *Inorg. Chem.* **1987**, *26*, 163–168; d) Z. Tian, D. G. Tuck, *J. Chem. Soc. Dalton Trans.* **1993**, 1381–1385; e) M. N. Gibbons, M. J. Begley, A. J. Blake, D. B. Sowerby, *J. Chem. Soc. Dalton Trans.* **1997**, 2419–2425.

[11] L. V. Gurevich, G. V. Karachenzev, V. N. Kondrat′ev, U. A. Lebedev, V. A. Medvedev, V. K. Potapov, U. S. Hodeev, *The Energy of Chemical Bonds Breaking. The Ionization Potentials and Electron Affinity*, Nayka, Moscow, **1974**, p. 351.

[12] a) V. L. Pecoraro, M. J. Baldwin, A. Gelasco, *Chem. Rev.* **1994**, *94*, 807–826; b) M. W. Urban, K. Nakamoto, F. Basolo, *Inorg. Chem.* **1982**, *21*, 3406–3408.

[13] S. S. Batsanov, *Russ. J. Inorg. Chem.* **1991**, *36*, 3015.

[14] J. Bordner, G. O. Doak, T. S. Everett, *J. Am. Chem. Soc.* **1986**, *108*, 4206.

[15] H. J. Breunig, T. Kruger, E. Lork, *J. Organomet. Chem.* **2002**, *648*, 209–213.

[16] F. H. Allen, O. Kennard, D. G. Watson, L. Brammer, A. G. Orpen, R. Taylor, *J. Chem. Soc. Dalton Trans.* **1987**, *12*, 1–18.

[17] S. Dutta, S.-M. Peng, S. Bhattacharya, *Inorg. Chem.* **2000**, *39*, 2231.

[18] a) J.-M. Aubry, C. Pierlot, J. Rigaudy, R. Schmidt, *Acc. Chem. Res.* **2003**, *36*, 668–675; b) M. Seip, H.-D. Brauer, *J. Am. Chem. Soc.* **1992**, *114*, 4486–4490; c) T. Sawada, K. Mimura, T. Thiemann, T. Yamato, M. Tashiro, S. Mataka, *J. Chem. Soc. Perkin Trans. 1* **1998**, 1369–1371.

[19] K. A. Kocheshkov, A. P. Skoldinov, N. N. Zemlyanskii, *Methods of Elementorganic Chemistry. Stibium and Bismuth*, Nauka, Moscow, **1976**, p. 483.

[20] G. A. Abakumov, N. O. Druzhkov, Yu. A. Kurskii, A. S. Shavyrin, *Russ. Chem. Bull.* **2003**, *112*, 712.

[21] A. I. Prokof′ev, V. B. Vol′eva, I. A. Novikova, I. S. Belostozkaya, V. V. Ershov, M. I. Kabachnik, *Russ. Chem. Bull.* **1980**, *89*, 2707–2710.

[22] D. D. Perrin, W. L. F. Armarego, D. R. Perrin, *Purification of Laboratory Chemicals*, Pergamon, Oxford, **1980**.

[23] G. M. Sheldrick, SADABS v. 2.01, Bruker/Siemens Area Detector Absorption Correction Program, Bruker AXS, Madison, Wisconsin, **1998**.

[24] G. M. Sheldrick. SHELXTL v. 6.12, Structure Determination Software Suite, Bruker AXS, Madison, Wisconsin, **2000**.

Received: December 8, 2005
Published online: March 7, 2006

